# R&D ROADMAP FOR TWO-PHASE THERMAL CONTROL SYSTEMS FOR PLANETARY BASE & SURFACE SYSTEMS APPLICATIONS

**A.A.M. Delil**
AATCS Consultants
Kaspischestraat 13, 8303EX Emmeloord, Netherlands
+31 (0)527 617576, adelil@xs4all.nl

**Abstract**

Discussed are critical theoretical and experimental R&D issues to be investigated for candidate two-phase thermal control systems (and their components), in order to define what is to be done to develop reliable systems, for near and far future planetary applications envisaged. Earlier publications SAE-2007-01-3242 and SAE-2008-01-2006 discuss that such advanced thermal control systems are one of the key technologies needed for future applications within the framework of the NASA Authorization Act 2005, specifying a programme to be established to develop sustained human presence on the Moon, including a robust pre-curser programme to promote exploration, science, commerce and US pre-eminence in space, also as a stepping stone to future exploration of Mars and many other planetary destinations. Results of these publications are briefly summarised, made more complete, and interesting thermal issues are added, resulting in a possible, long-term R&D roadmap.

**KEYWORDS**

Thermal Control Systems, Two-Phase Thermal Control, Planetary Applications, Planetary Exploration/Science/Commerce, Planetary Surface Systems, Environmental Moon & Mars Issues, Moon & Mars Base, R&D Roadmaps, Thermal Gravitational Modelling & Scaling, Π-Numbers, Two-Phase Loops, Electro-Osmosis, Electro-Hydro-Dynamics, Electro-Wetting, Flow Regimes & Flow Pattern Mapping, Rotating Heat Pipe Joint, Vapour Pressure Driven Heat Transfer Devices, Pulsating/Oscillating Heat Transfer Devices

## INTRODUCTION

The US vision for space exploration includes [1]: Completion of the International Space Station and safely flying the Space Shuttle until 2010, developing, flying the Crew Exploration Vehicle no later than 2014 (goal 2012), return to the Moon no later than 2020 and extending human presence across the solar system and beyond, implementing a sustained and affordable human and robotic program, development of supporting innovative technologies, knowledge and infrastructures, promotion of international & commercial participation in exploration.

As a consequence of this vision, the NASA Authorization Act 2005 states that the Administrator shall establish a programme to develop a sustained human presence on the Moon, including a robust pre-curser programme to promote exploration, science, commerce and US pre-eminence in space, and as a stepping stone to future exploration of Mars and other destinations. This first step is to be done for regaining and extending operational experience in hostile planetary environments, developing capabilities needed for to open the space frontier and to prepare human operation on Mars and for science operations and discovery. The next step is to fulfil the human destiny as explorers.

NASA's Exploration Roadmap (Fig. 1) and Exploration Technology Roadmap (Fig. 2) clearly depict an overview of the work to be done. Further details on program constellation components [1] pertain to the Lunar exploration architecture, CEV (Crew Exploration Vehicle, Orion), Crew & cargo launch vehicles, LSAM (Lunar Surface Access Module), Possible South Pole Outpost, Safe, Accelerated, affordable, sustainable approach, Lunar pre-cursor and robotic program, Commercial orbital transportation services, Exploration program status, Key technologies needed (Fig. 3), and Exploration Technology development Program.

Key technologies, needing further development, include thermal management systems for Moon and Mars base household (habitability) and science applications. Very promising planetary thermal management systems are two-phase thermal control systems: Capillary Pumped Loops, Loop Heat Pipes, Vapour Pressure Driven Loops, Mechanically Pumped Loops (in series, parallel, hybrid configuration) and Vapour Compression Systems. The starting-point is that planetary two-phase

thermal control systems can be properly developed, using experimental results of terrestrial scale-model systems, built according to thermal-gravitational modelling and scaling laws [2].

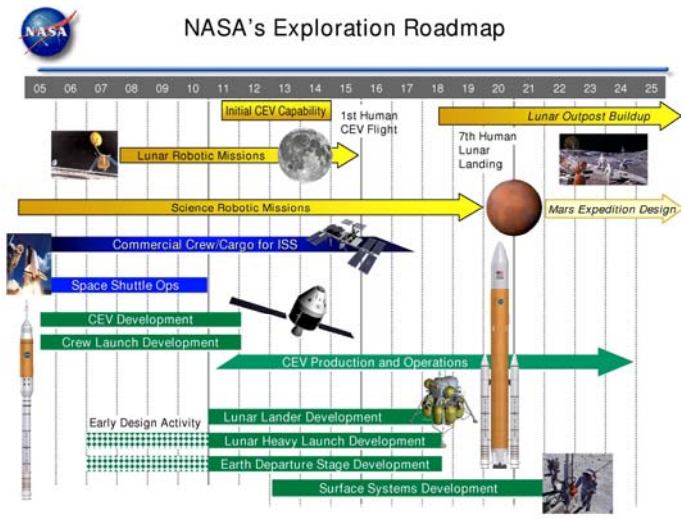


Fig. 1. NASA Exploration Roadmap [1]

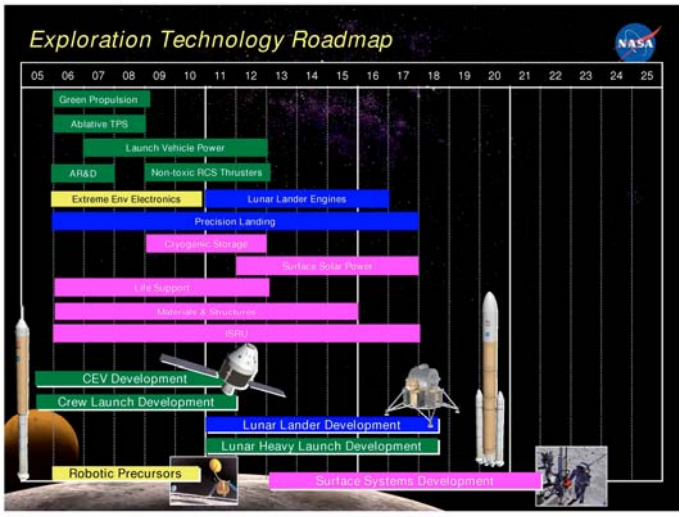


Fig. 2. NASA Exploration Technology Roadmap [1]

## STARTING-POINT SUMMARY

The thermal-gravitational modelling & scaling approach, described in [2] and its references [3-8], is based on similarity considerations [9], which led to the identification of 18 dimensionless numbers (called π-numbers). The 18 numbers, listed in the first column of Table 1, are crucial for the thermal gravitational scaling of two-phase thermal control systems. The other columns show the different sections of the two-phase heat transport system, schematically depicted in Figure 4: Pure liquid lines (with and without heat exchange), capillary or swirl evaporators, vapour lines, two-phase lines and condensers indicates whether a π-number is relevant in a particular section.

The relevant equation

$$(1 - \alpha)/\alpha = S(\rho_v/\rho_l)X/(1 - X) \qquad (1)$$

relates vapour quality X and volumetric vapour (void) fraction) α, and (combinations of) π-numbers chosen.

The Morton number Mo

$$\pi_{15} = Mo_l = Re_l^4 Fr_l/We^3 = \rho_l \sigma^3/\mu_l^4 g \qquad (2)$$

is useful for scaling two-phase flow with respect to gravity, as it contains only liquid properties, surface tension and gravity

The Mach number Ma:

$$\pi_{16} = Ma = v/(\partial p/\partial \rho)^{1/2} \qquad (3)$$

crucial if compressibility is important, as choking depends on the two-phase mixture vapour quality.

The enthalpy or boiling number

$$\pi_{14} = Boil = \Delta H(z)/ h_{lv} = Q/\dot{m}.h_{lv}. \qquad (4)$$

Q is the power fed to the boiling liquid. This number appears in the dimensionless enthalpy expression at any z in a line heated from outside (q is the heat flux):

$$\pi_{14} = \Delta H(z)/h_{lv} = \Delta H_{in}/h_{lv} + \pi Dzq/\dot{m}h_{lv}. \qquad (5)$$

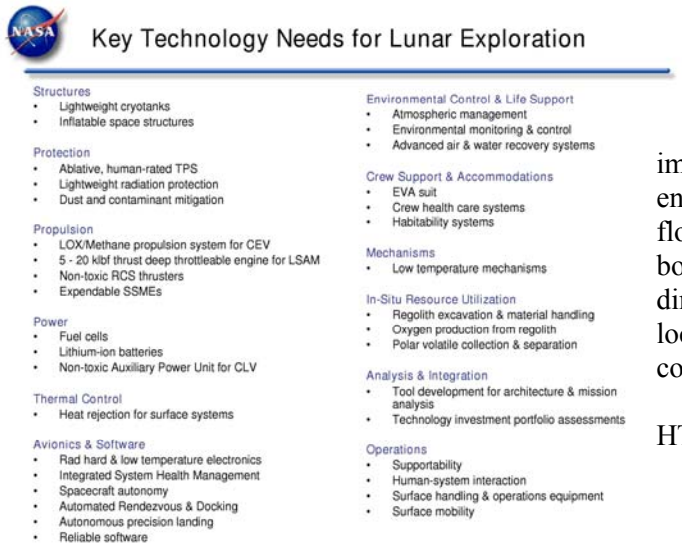


Fig. 3. Key Technology Needs [1]

For sub-cooled or heated liquid this is

$$\pi_{14} = Q/\dot{m}\, Cp_l \Delta T. \qquad (6)$$

$\Delta T$ is the temperature drop. The above implies that, if dimensionless entrance enthalpies are equal for different fluids flowing in a similar geometry, equality of the boiling number ensures equal non-dimensional enthalpy at similar axial locations, hence equal qualities, similar sub-cooling & boiling lengths.

The condensation number, h is the local HTC,

$$\pi_{17} = (h/\lambda_l)\,(\mu_l^2/g\,\rho_l^{\,2})^{1/3}. \qquad (7)$$

The vertical wall condensation number ($T_o$ is the local sink, T is the local saturation temperature:

$$\pi_{18} = L^3\rho_l^2\, g\, h_{lv}/\mu_l \lambda_l (T - T_o). \qquad (8)$$

Table 1. Relevance of π-numbers for thermal gravitational scaling of two-phase loops

| Relevant π-numbers for the thermal-gravitational scaling of two-phase loops | Liquid Sections | | Evaporators Swirl/Capillary | Vapour and 2-Phase lines | Condenser |
|---|---|---|---|---|---|
| | Adiabatic | Heating/Cooling | | | |
| $\pi_1 = D/L$ = geometry | • | • | • | • | • |
| $\pi_2 = Re_l = (\rho v D/\mu)_l$ = inertia/viscous | • | • | • | • | • |
| $\pi_3 = Fr_l = (v^2/gD)_l$ = inertia/gravity | • | • | • | /• | • |
| $\pi_4 = Eu_l = (\Delta p/\rho v^2)_l$ = pressure head/inertia | • | • | • | • | • |
| $\pi_5 = \cos \nu$ = orientation with respect to g | • | • | • | /• | • |
| $\pi_6$ = S = slipfactor = $v_v/v_l$ | | | • | • | • |
| $\pi_7$ = density ratio = $\rho_v/\rho_l$ | | | • | • | • |
| $\pi_8$ = viscosity ratio = $\mu_v/\mu_l$ | | | • | • | • |
| $\pi_9 = We_l = (\rho v^2 D/\sigma)_l$ = inertia/surface tension | | | • | /• | • |
| $\pi_{10} = Pr_l = (\mu Cp/\lambda)_l$ | | • | • | | • |
| $\pi_{11} = Nu_l = (hD/\lambda)_l$ = convective/conductive | | • | • | | • |
| $\pi_{12} = \lambda_v/\lambda_l$ = thermal conductivity ratio | | | • | | • |
| $\pi_{13} = Cp_v/Cp_l$ = specific heat ratio | | | • | | • |
| $\pi_{14} = \Delta H/h_{lv}$ = Bo =enthalpy nr. X=quality | | • | • | • | • |
| $\pi_{15} = Mo_l = (\rho_l\sigma^3/\mu_l^4\, g)$ = capillarity/buoyancy | | | • | /• | • |
| $\pi_{16} = Ma = v/(\partial p/\partial\rho)^{1/2}{}_s$ | | | • | • | • |
| $\pi_{17} = (h/\lambda_l)(\mu_l^2 g)^{1/3}$ | | | • | | • |
| $\pi_{18} = L^3\rho_l^2\, g\, h_{lv}/\lambda_l\mu_l(T - T_o)$ | | | • | | • |

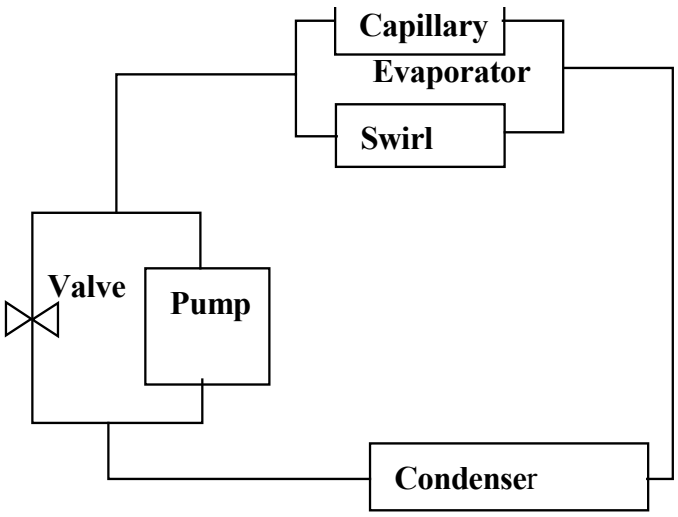


Fig. 4. Schematic of Two-Phase Loop

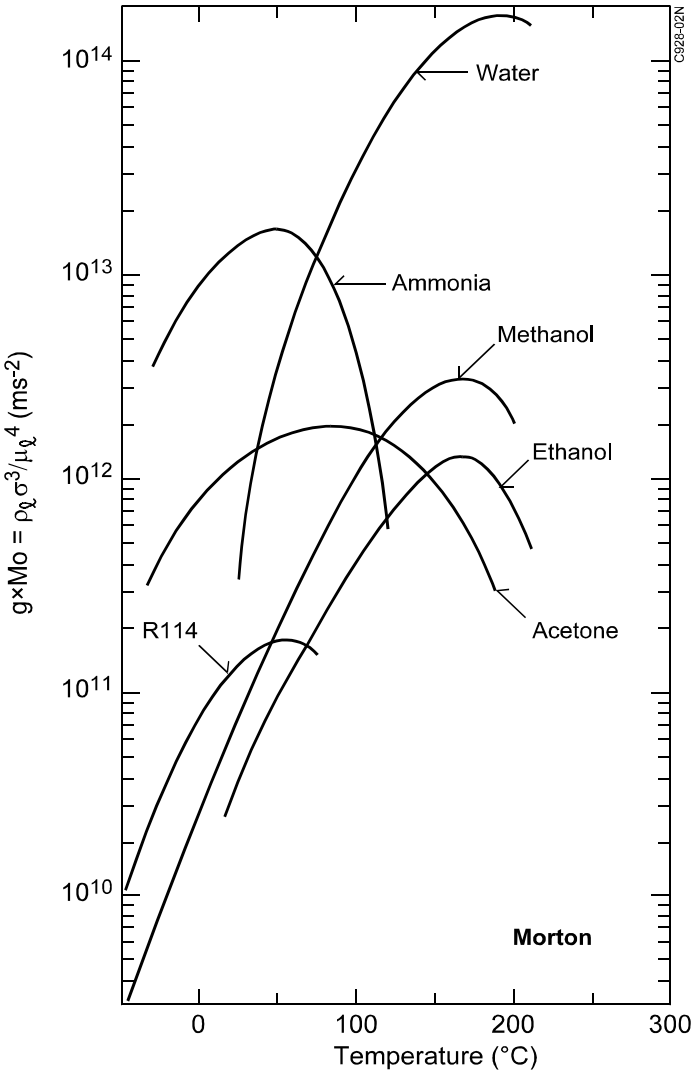


Fig. 5. $\rho_l.\sigma^3/\mu_l^4$ versus temperature, for some fluids

A relatively simple and very attractive scaling possibility is the scaling of a two-phase prototype for a Mars and a Moon base, by a terrestrial model with the same or a scaled working fluid. As the ratio of gravity levels between prototype and model is less than 1 decade (Mars gravitation ~ 0.4-g, Moon gravitation ~ 0.16-g), the sizes of the model have to be only slightly larger than the geometric sizes of the prototype. In addition, adjustment of the inclination (cos ν) of non-horizontal lines in the terrestrial (1-g) model may help to realise almost perfect scaling. The ammonia curves in Figure 5 show that for perfect scaling (Mo must be equal for the 0.4-g Mars prototype and for the terrestrial model), that the value of $(\rho_l.\sigma^3/\mu_l^4)_{0.4\text{-g prototype}}$ must be 0.4 times the value of the terrestrial model $(\rho_l.\sigma^3/\mu_l^4)_{1\text{-g model}}$. Choosing say $4 \cdot 10^{12}$ for Mars prototype at a testing temperature of say –20 °C, means for the terrestrial model $10^{13}$ a test temperature of roughly +10 °C. Figure 6 now simply yields the geometric scaling factor by dividing the ammonia ordinate value at –20 °C for the Mars prototype (0.0070), by the ordinate value at +10 °C for the terrestrial model (0.0067), being approximately 1.05. Consequently, as the We/Fr is to be the same in model and prototype $1.05 \sim (D \cdot g^{1/2})_{prototype} / (D \cdot g^{1/2})_{model}$, yielding $(D_{model} / D_{prototype}) = (L_{model} / L_{prototype}) = (1.05)^{-1}.(0.4)^{1/2} \approx 0.6$. In other words, thermal-gravitational scaling of an ammonia full-scale Mars prototype can simply be realised via a pure geometrically scaled terrestrial ammonia model system, having acceptable dimensions, i. e. ~ 60% of the Mars prototype dimensions.

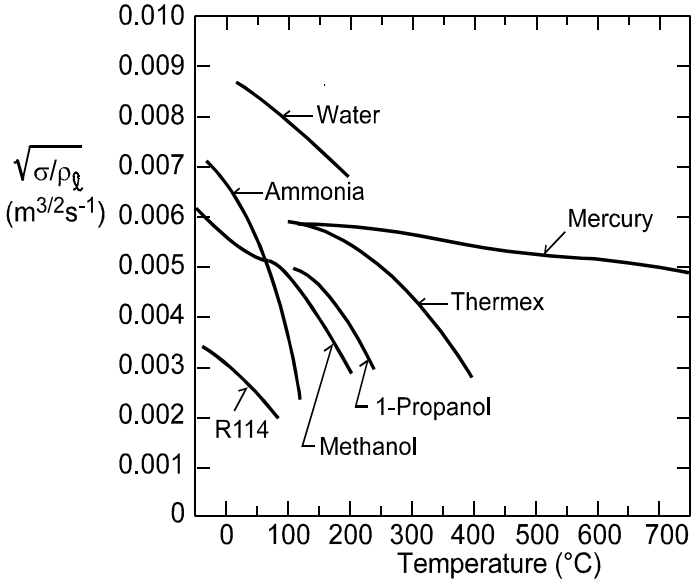


Fig. 6. $(\sigma/\rho_l)^{1/2} = D.g^{1/2}.(We/Fr)^{-1/2}$ versus temperature, for various working fluids.

For ammonia and some other candidate working fluids in the thermal control range for Mars and Moon applications (methanol, acetone and R114), the same exercises are currently being repeated for the terrestrial scaling to Mars and Moon gravity conditions. Results will in detail be discussed in September 2008 [10]. Anticipating that data from experiments with a simple pre-cursor system on the Moon surface will be available before a pre-cursor test system will be built and sent to Mars, the case of scaling between Moon and Mars gravity levels is included in the discussion. The exercise outcomes tell us that geometric model sizes will be (within an acceptable ratio) smaller than the geometric sizes of (pre-cursor) prototypes [10].

## DEVELOPMENT SUPPORT FINETUNING

Once having defined the features of the model and prototype systems, activities are to be carried out to support and fine-tune the thermal-gravitational design of two-phase thermal control systems for Moon and Mars applications. These supporting activities pertain to the experimental determination of flow pattern maps for different g-levels and the writing down of the constitutive equations for two-phase fluid flow and heat transfer for the all flow patterns in each section of both systems.

An important conclusion to be drawn first, is: Condensers and, in mechanically pumped systems, also two-phase lines, are crucial in scaling with respect to gravity. They set conditions for evaporators and single-phase sections. A second conclusion is: In adiabatic two-phase lines of mechanically pumped systems in low-gravity, only shear forces will cause separation of phases in a high-quality mixture. This leads to annular flow (a fast moving vapour in the core and a, by frictional drag induced, slowly moving liquid annulus at the inner line wall) for the lower flow rates. For increasing power, hence flow rate, the slip factor will increase introducing waves on the liquid-vapour interface and entraining of liquid droplets in the vapour: wavy-annular-mist flow. A similar flow pattern can be predicted for vertical downward flow on earth, as it easily can be derived from the flow pattern map for downward two-phase flow shown in Fig. 7. The two-phase flow Froude number used in this figure is:

$$Fr_{tp} = (16\,\dot{m}^2/\pi^2 D^5 g) \times \times [X^2/\rho_v^2 + (1-X)^2/\rho_l^2]. \qquad (10)$$

Comparing low-g and vertical downward terrestrial flow one has to account in the latter for the reduction of the slip factor by the gravity forces assisting the liquid layer flowing down (draining effect). Anyhow, vertical down flow is the preferred two-phase line orientation in the terrestrial model, because of its axial-symmetric flow pattern. A similar conclusion can be drawn for the straight tube condenser. In condensers the flow will change from wavy annular mist to pure liquid flow, passing several flow patterns, depending on the path of the condensation.

### Pressure drop & heat transfer equations

As two-phase sections are considered to be crucial for two-phase loop modelling and scaling, the following considerations will focus on pressure drops in condensing and adiabatic flow. The discussion is restricted to straight tubes, with a constant circular cross-section.

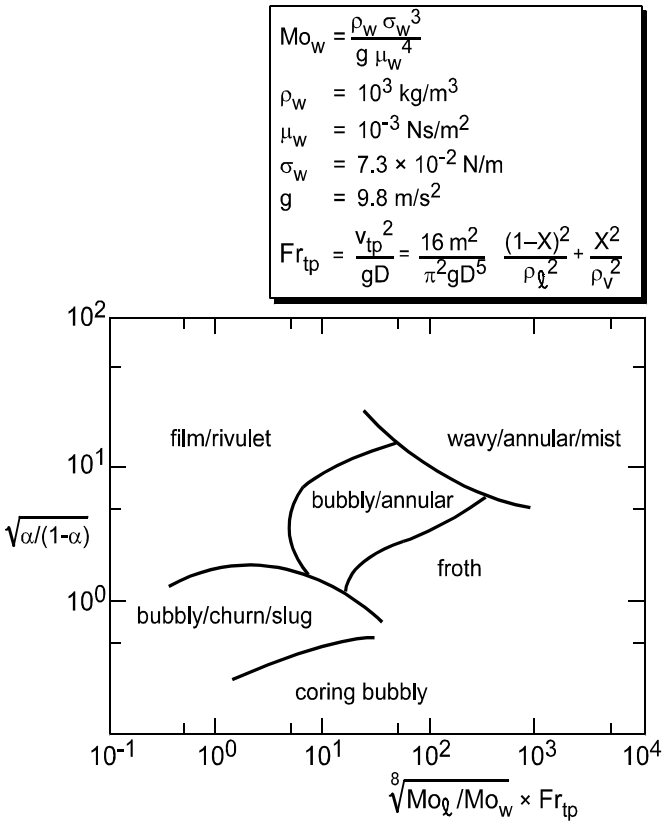


Fig. 7. Flow pattern map (vertical down flow) [11]

The total local pressure gradient for annular flow $(dp(z)/dz)_t$ is the sum of the friction, the momentum and the gravity gradient.:[12-14], the contribution of friction (deleting the z-dependence to shorten the notation) is:

$$(dp/dz)_f=(32m^2/\pi^2\rho_v D^5)(0.045/Re_v^{0.2})[X^{1.8}+ +5.7(\mu_l/\mu_v)^{0.0523}*(1-^{.47}X^{1.33}(\rho_v/\rho_l)^{0.261}+ +8.1(\mu_l/\mu_v)^{0.105}*(1-X)^{0.94}X^{0.86}(\rho_v/\rho_l)^{0.522}]. \quad (11)$$

X is local quality X(z). $Re_v$ is the Reynolds number,

$$Re_v = 4m/\pi D\mu_v. \quad (12)$$

Fluid properties are assumed independent of z, since they depend only on the mixture temperature, which usually is almost constant in adiabatic and condensing sections.

The momentum constituent can be written as

$$(dp/dz)_m=-(16m^2/\pi^2D^4)\{[2X(1-\alpha)/\rho_v\alpha^2 - \beta(1-X)/\rho_l\alpha + + (1-\beta)(1-X)/\rho_l(1-\alpha)+(1-X)/\rho_l(1-\alpha)](dX/dz) + + [X^2(1-\alpha)/\rho_v\alpha^3+(1-X)^2/\rho_l(1-\alpha)^2](d\alpha/dz)\} \quad (13)$$

Here α is the z-dependent local void fraction α(z), β = 2 for laminar liquid flow, 1.25 for turbulent flow.

The gravity constituent is

$$(dp/dz)_g = (1-\alpha)(\rho_l - -\rho_v)g\cos\nu. \quad (14)$$

$g \to 0$ for microgravity conditions and g cosν equals 9.8 m/s$^2$ for vertical down flow on Earth, 3.74 m/s$^2$ for vertical down flow on Mars and 1.62 m/s$^2$ on the Moon. α is eliminated in (13) and (14) by inserting (1).

Slip factor S is to be specified. The principle of minimum entropy production [15] yields

$$S =[(1+1.5Z)(\rho_l/\rho_v)]^{1/3} \quad (15)$$

This is for annular flow, in which the constant Z (according to experiments) is above 1 and below 2.

$$S = \{(\rho_l/\rho_v)[1+Z'(\rho_v/\rho_l)(1-X)/X]/[1+Z'(1-X)/X]\}^{1/3} \quad (16)$$

for real annular-mist flow, annular flow with a mass fraction Z' of liquid droplets entrained in the vapour. Z' is between 0 (zero entrainment) and 1 (full entrainment). In the limiting cases $Z \to 0$ and $Z' \to 0$, (15) and (16) reduce to

$$S = (\rho_l/\rho_v)^{1/3} \quad (17)$$

This represents ideal annular flow. It will be used here for simplicity reasons and since it allows comparison with the results of calculations found in literature. The influence of $Z \neq 0$ and $Z' \neq 0$ is interesting for future investigations.

Inserting (17) into (1) and (11), (13), (14), yields

$$(dp/dz)_m = -(32\,m^2/\pi^2\rho_v D^5) \times \times (D/2)(dX/dz)\,[2(1-X)(\rho_v/\rho_l)^{2/3} + +2(2X-3+1/X)(\rho_v/\rho_l)^{4/3} + (2X-1 - - \beta X)(\rho_v/\rho_l)^{1/3} + (2\beta - \beta X - - \beta/X)(\rho_v/\rho_l)^{5/3} \times +2(1-X-\beta + \beta X)(\rho_v/\rho_l)]. \quad (18)$$

$$(dp/dz)_g = (32m^2/\pi^2\rho_v D^5)\{1 - - [1+(\rho_v/\rho_l)^{2/3}\,(1-X)/X]^{-1}\} \times \times [\pi^2 D^5 g\cos\nu(\rho_l - \rho_v)\rho_v/32m^2]. \quad (19)$$

To solve (11), (18, (19) an extra relation is necessary, defining the z-dependence of X. Often used is

$$dX/dz = -X_{entrance}/L_c, \quad (20)$$

$L_c$ = condensation length). It means unrealistic uniform heat removal, and linear quality decrease along the duct. It is better to use

$$\dot{m}\, h_{lv}(dX/dz) = -h\pi D[T(z)-T_s], \qquad (21)$$

relating the local vapour quality and heat transfer. h is the local heat transfer coefficient h(z), for which we can write

$$h = 0.018(\lambda_l\rho_l^{1/2}/\mu_l)Pr_l^{0.65}|-(dp/dz)_t|^{1/2}\, D^{1/2}, \qquad (22)$$

assuming that the major thermal resistance is in a laminar sub-layer of the turbulent condensate film.

As already mentioned the two-phase flow path is almost isothermal, which implies constant temperature drop $T(z) - T_s$ (for a constant sink temperature $T_s$), constant fluid properties and a constant Prandtl number, being

$$Pr_l = Cp_l\, \mu_l\, /\lambda_l. \qquad (23)$$

The total condensation pressure drop is

$$\Delta p_t = \int_0^{L_c} (dp/dz)_t dz. \qquad (24)$$

The equations (1), (11), (18)–(22) can be combined. This yields an implicit non-linear differential equation in the variable X(z), which can be rewritten into a solvable standard form for differential/algebraic equations

$$F(dX/dz, X) = 0. \qquad (25)$$

Figure 8 compares pressure gradient constituents for ammonia vertical down-flow at two temperatures. The curves prove that the impact of gravity decreases with decreasing temperature. This confirms the statement that low-gravity behaviour can be simulated the best by terrestrial down-flow tests at low temperature.

Modelling calculations were extended from adiabatic to condensing flow in a straight duct [11, 12] to investigate the impact of gravity level on the duct length required to achieve complete condensation. This impact, reported to lead to duct lengths being more than one order of magnitude larger for zero gravity, as compared to horizontal orientation on earth [16], was assessed for various mass flow rates, duct diameters and thermal (loading) conditions, for ammonia and R114.

A summary of results of calculations for ammonia is presented next. To compare the results of calculations with data from literature, the condenser of [16] was chosen as the baseline. Main characteristics are: Power 1 kW, line diameter 16.1 mm, ammonia temperature 300 K and temperature drop to sink 10 K. The gravity levels considered are: zero gravity, Earth-g = 1-g = 9.8 m/s$^2$, Mars-g = 3.74 m/s$^2$, Moon-g = 1.62 m/s$^2$, and 2-g super-g = 19.6 m/s$^2$.

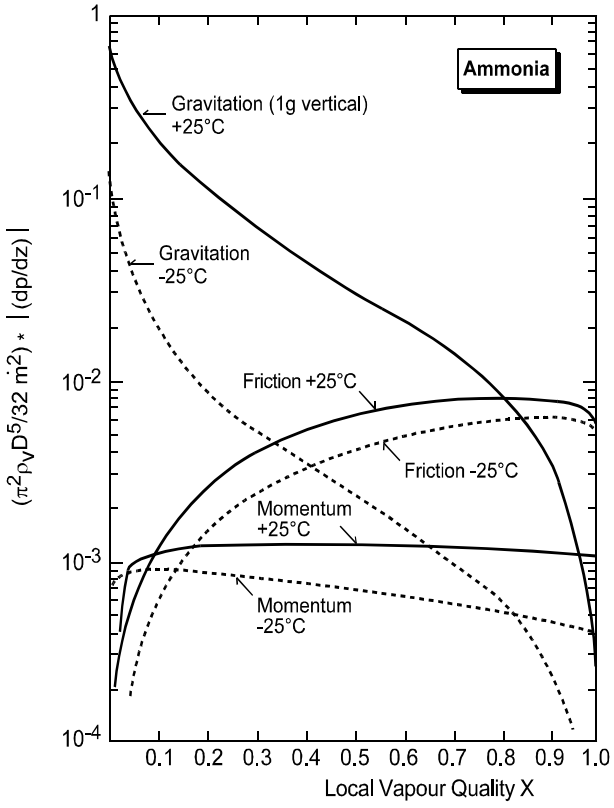


Fig. 8. Pressure gradient constituents as function of vapour quality, for ammonia at +25 and –25 °C

Illustrative results of calculations, given in Figure 9, depict the vapour quality X along the condensation path as a function of non-dimensional length z/D, for all gravity levels mentioned, including the curves for 0-g and for horizontal condensation on earth, found in [16]. From the figure it can be concluded that the length required for full condensation strongly increases with decreasing-g. 0-g condensation length is ~ 10 times the 1-g length. Data of [16] are to extreme.

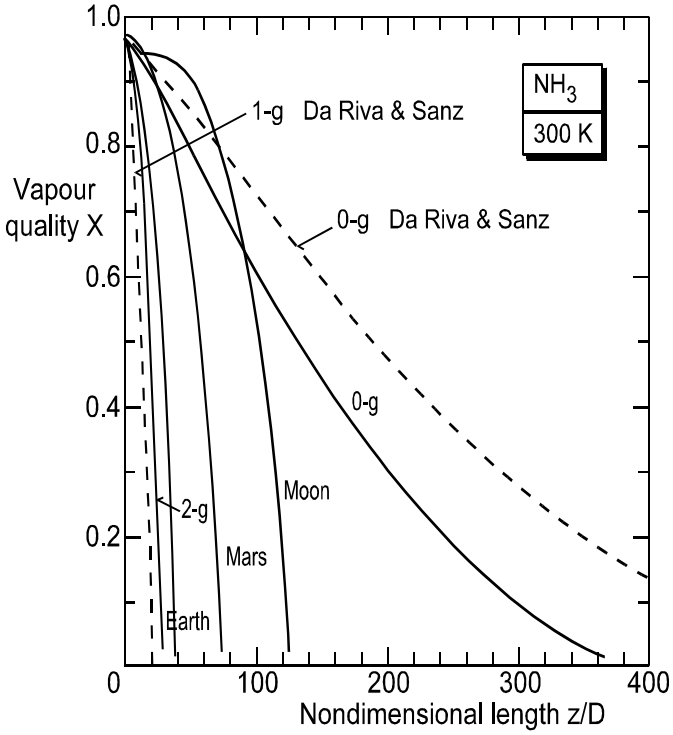


Fig. 9. Vapour quality along the reference duct [16]

To assess the impact of the saturation temperature on condensation, similar curves were calculated for two other temperatures, 243 K and 333 K, and the above parameter values. These curves indicate that the full condensation length increases with temperature for zero-g conditions, but decreases with temperature for other gravity levels [13, 14]. This implies that differences between 1 – g and Mars & Moon-g's decrease with decreasing temperature.

Calculations of the vapour quality distribution along the 16.1 mm reference duct for condensing ammonia (at 300 K) under 1-g and lower than 1-g conditions, for power levels ranging from 0.5 kW up to 25 kW, yielded that:

Power from 25 kW down to 500 W, corresponds in lower than 1 – g conditions to relatively minor full condensation length reductions. Power and length are strongly related: From 554 D down to only 19 D.

The g-dependence of the full condensation lengths decrease with increasing power, until differences vanish condenser choking conditions for all flow patters. The latter value is upper limit for ideal annular flow [13, 14].

Calculations of the vapour quality along the duct, for 0-g and 1-g and three duct diameters (8.05, 16.1, 24.15 mm) at 300 K, show that the ratio between full condensation lengths in 0-g and 1-g ranges from say 1.5 for the 8.05 mm duct to over 30 for the 24.15 mm duct: Small line diameter systems are less sensitive, for differences in g-levels, than large diameter ones. TPX I flight data confirmed this [17].

**Flow pattern issues**

As the model developed is mainly valid for annular flow, it will be worthwhile to investigate the impact of other flow patterns inside the condenser duct (mist flow at high quality, slug and bubbly flow at low quality and wavy-annular-mist in between). Hence it is to investigate whether the pure annular flow assumption, leads towards substantially overestimated full condensation lengths. Complications are that the boundaries flow patterns are not accurately known and flow pattern transitions strongly depend on temperature and line diameter. Accurate knowledge of the gravity level dependent two-phase flow regimes is crucial for modelling and designing two-phase heat transport systems for space, as flow patterns directly affect thermal hydraulic characteristics of two-phase flow and heat transfer [19,20]. Therefore flow pattern (regime) maps are to be created, either in non-dimensional format (Fig. 7), 2D-format (Fig. 10, [18]), or 3D-format (Fig. 11). The latter figure presents data measured during many, many K135 aircraft flight trajectories, in $10^{-2}$-g, Mars-g, Moon-g and 1-g [18]. Such flow pattern maps can then be used to determine, in an iterative way, via the flow pattern dependent constitutive equations for two-phase flow and heat transfer, the actual trajectories of condensing and evaporating (boiling) flow. The latter will finally lead to an accurate determination of the pressure drops in the various sections and of the heat transfer in the evaporator or condenser sections of a two-phase heat transport system, as pressure drops strongly depend on the flow patterns within the trajectory (Fig. 10).

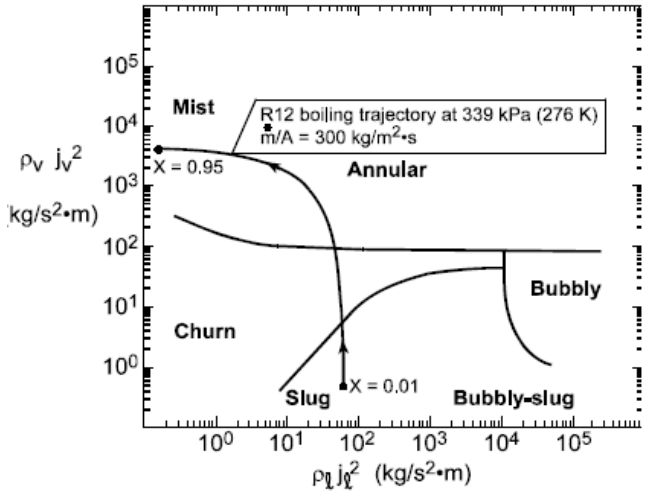


Fig. 10.1 – g Vertical Flow Boiling Regime Map [18]

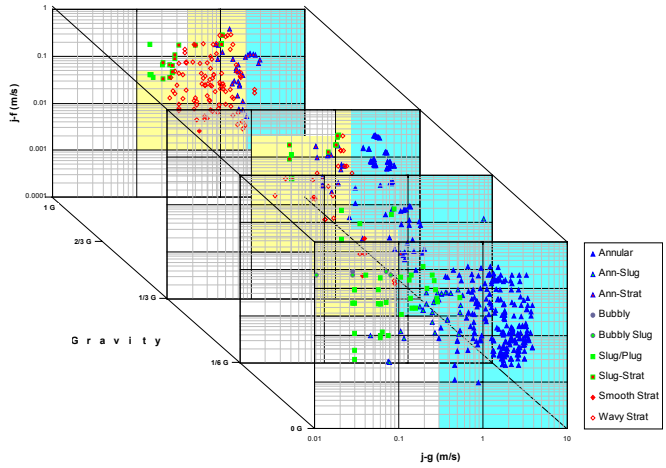


Fig. 11. 3-Dimensional Flow Regime Map [19]

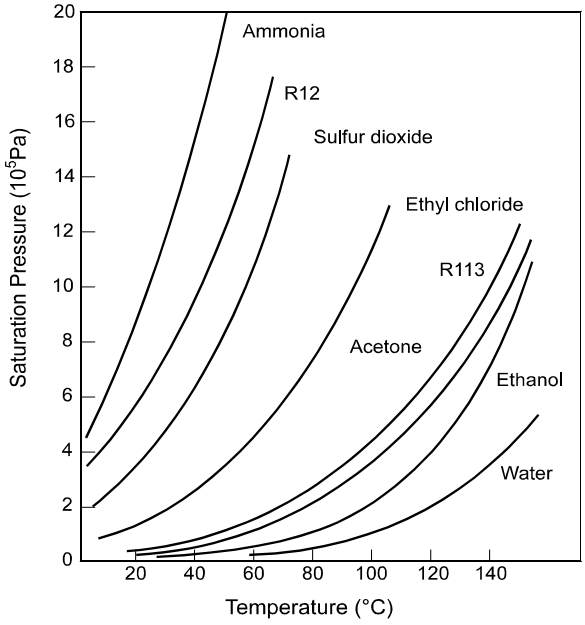


Fig. 12. Saturated Pressure versus temperature for various working fluids

It is stressed that to realise this the pressure drop and heat transfer equations are to be written down for all flow patterns: A huge effort, which can be based on excellent handbooks, e. g. [20].

All remarks made so far are valid for all types of two-phase heat transfer loops, including pulsating two-phase loops, whose operation is driven only by vapour pressure built-up, induced by the heat to be transported itself and controlled by two one-way valves, one at the inlet, the other at the outlet of the evaporator [21–23]. These loops do not need an additional power source. The only new issue is the proper design of the working fluid dependent driving pressure, which is set by the saturated temperature difference between evaporator and condenser (Fig. 12).

**R&D trajectory to be followed**

A trajectory to develop two-phase systems for planetary applications starts with thermal-gravitational modelling and scaling, between Earth-g and Moon-g (1-g → 0.16-g). This is followed by thermal-gravitational modelling & scaling between Earth-g and Mars-g (1-g → 0.4-g) and between Moon-g and Mars-g ((0.16-g → 0.4-g).

In parallel are many more 1-g, 0.4-g and 0.16-g flow pattern data still to be collected, for all candidate working fluids, by KC135 flights [18] and during by experiments in Maglev, JPL's magnetic levitation test bed [24]: A users facility accommodating long-duration experiments/ tests in variable gravities, on large samples or scaled devices (Fig. 13). It can simulate g-levels on the moon and other planets for most thermal control liquids, e. g. oxygen, hydrogen, nitrogen, ammonia, water, methane, ethane, acetone, and other refrigerants.

Maglev applications include the study of:

Experimental thermal fluid physics, where gravity is an important parameter. g-effects on pool boiling and two-phase flow in model systems, high flux heat transfer in pool & flow boiling. Testing and optimisation of space-borne thermal fluid devices for thermal control, life support, and resource utilization, e. g. heat pipes, phase separators, cooling loops, cryogen transfer and propellant supply in space.

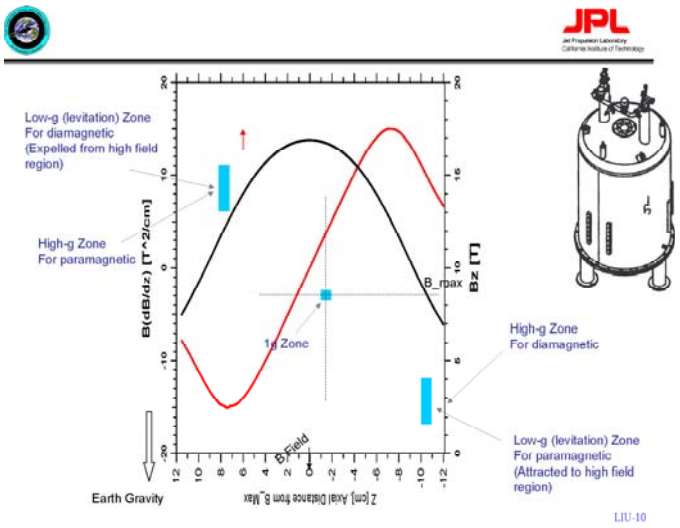


Fig. 13. Maglev, Levitation Zones for Large Bore [24]

Briefly said: The Maglev test bed can deliver useful contributions to other flow pattern collection activities and contribute to development of loops/ components.

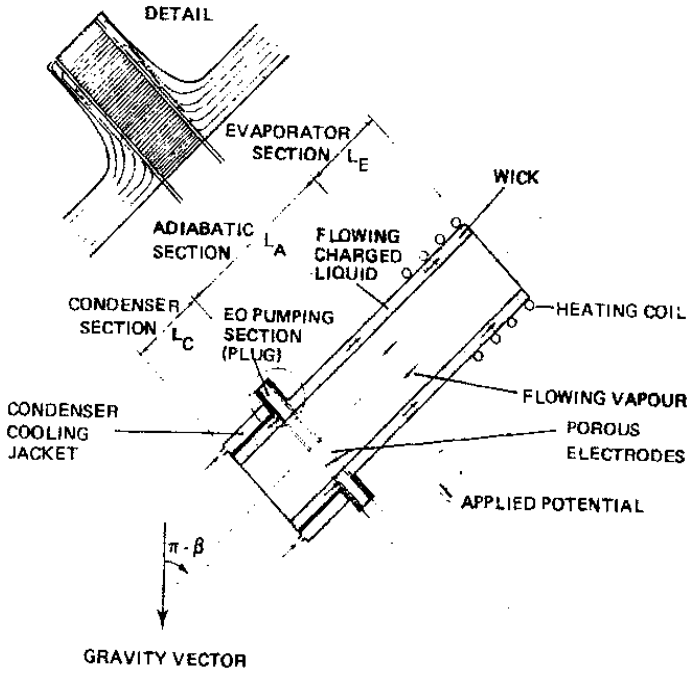


Fig. 14. Schematic of EOHP with a short electro-osmotic pumping section (plug) [29]

As said before, also constitutive modelling equations are to be derived for all flow patterns, working fluids, g-levels and inclinations with respect to g, system diameters, etc. This must finally lead to developing the pre-cursor test system to collect real Moon data first. These data shall be the baseline for the development of the real Moon TC system prototype and of pre-cursor test system to collect real data on Mars. Data of the latter Mars system and of the real Moon TC system will lead to the realisation of the real Mars system to be launched.

## ADDITIONAL R&D ISSUES

It is considered worthwhile [25-28] to do additional R&D, in parallel to the described R&D trajectory, to anticipate problems that might pop-up in the near future. Examples of problems pertain to boundary conditions for power, consumption versus availability, degradation of radiators (by dust or radio active particles), lifetime (wear of mechanical pumps, fatigue in flexible thermal joints, etc.). Some issues are briefly discussed below. They deal with alternative ways of controlled pumping (EO, EHD and EW) and the moveable thermal joint issue.

### Electro-Osmotic pumping and control

A fully controllable variable conductance electro-osmotic heat pipe (EOHP), containing a short electro-osmotic pumping section (Fig. 14), was created two decades ago. But this NLR development [29] was stopped, since electrode degradation unacceptably reduced lifetime. Nowadays EO-pumps are available, e.g. [30] or search the text "EO Pump" on Internet (via Google/Yahoo/etc.).

The principle of electro-osmotic pumping obeys the Onsager equations, describing the transfer from mechanical into electrical energy, respectively from electrical into mechanical energy:

$$\Delta p = R_f . \Phi + H.I$$

and $$\Delta V = H.\Phi + R_e .I \qquad (26)$$

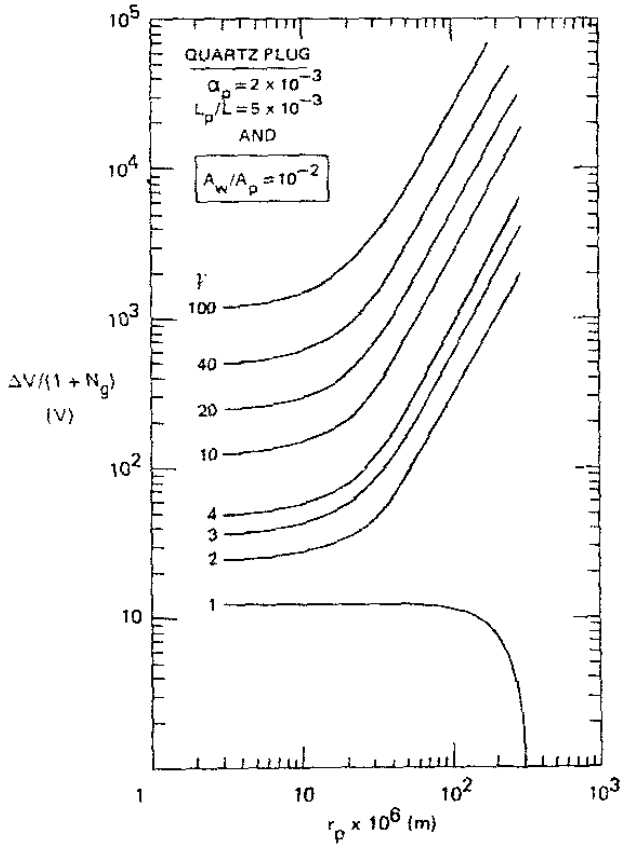


Fig. 15. $\Delta V/(1+N_g)$ versus enhancement factor $\gamma$ an pore radius, for water and the plug specified

$\Delta p$ is the pressure head, $\Delta V$ is the voltage drop, $\Phi$ is the liquid flow rate, I is the electric current, $R_f$ is the flow resistance, $R_{el}$ is the electric resistance, H is the Onsager coupling factor. The governing equations are:

$$Q_{el} = (\varepsilon_{plug} A_{plug}/L_{plug})(\lambda_{el\text{-}liq} + 2\lambda_{el\text{-}surface}/r_{plug})(\Delta V) \quad (27)$$

$$\gamma = Q/Q_{ref} = N_l N_w N_r (1+N_g+N_{eo})/[N_l N_w (1+N_g)] = N_r[1+N_{eo}/(1+N_g)] \quad (28)$$

$$N_r = 1/\{(1+ L_{plug}/L)[-1+K_w A_w/(K_{plug} A_{plug})]\} \quad (29)$$

$$N_w = 2K_w A_w/(L r_w) \quad (30)$$

$$N_l = \sigma \rho_l h_{lv}/\mu_l \quad (31)$$

Inserting all material values one obtains Figure 15, depicting $\Delta V/(1 + N_g)$ versus enhancement factor $\gamma$ and pore radius, for water and the quartz plug specified. Figure 15 shows the potential of the pumping enhancement and flow control of an EOHP with a short pumping section. This pumping section is an electro-osmotic pump (without moving parts), which can be applied not only in heat pipes, but also in two-phase thermal control loops. Flow control is by controlling $\Delta V$.

**EHD pumping and control**

Decades ago one unsuccessfully tried to develop EHD heat pipes, because of electrical breakdown due to the high voltages to be applied to get things working. But recently one succeeded at NASA-GSFC [31] to develop EHD-driven two-phase loops to study EHD pumping mechanisms for EHD TC systems for laser cooling application, for source-integrated micro-cooling devices, and for chip-integrated, EHD-pumped cryogenic cooling systems being developed.

Like EO, also EHD-pumped systems advantages are: No moving parts, low mass, low power consumption, low acoustic noise production, the need of a simple control system. A disadvantage is the high voltages needed for operation, except for small-scale systems.

Three terms contribute to the equation, governing EHD-pumping in the electric field direction,

$$F_{EHD} = \rho_c E - \tfrac{1}{2} E^2 \nabla \varepsilon + \tfrac{1}{2} \nabla [\rho E^2 (\delta\varepsilon/\delta\rho)_T] \quad (32)$$

The first represents the Coulomb force (forcing the liquid to move in the direction of the applied electric field, by ion-drag or pure conduction), the second is a di-electro-phoretic force, the third an electrostriction force.

The requirements for the laser cooling two-phase thermal control system, applied heat flux 25 W/cm$^2$ at an operating temperature of 20 °C. This led to the choice of a pure conduction EHD loop, using HCFC 134A as the working fluid. Conduction pumping has the advantage that there is no ions-injection, hence no fluid degradation, and that attainable pressure heads are higher than the heads attainable with other EHD pumping techniques. Figure 16 shows some experimental results obtained for a micro-scale TCl system ion-drag pump.

Concerning EHD for laser cooling it was concluded that:

– Both two-phase operation up to 35 W/cm$^2$ and dry-out recovery (by simply increasing the applied voltage) have been demonstrated.
– Pump performance with fluid properties and operating temperature has been characterised.
– Power consumption has been quantified.

For the micro-scale TC system ion drag pumping has been proven to be successful, but as results are not always consistent and pumping capability is limited, a loop with a pure conduction pump has been developed.

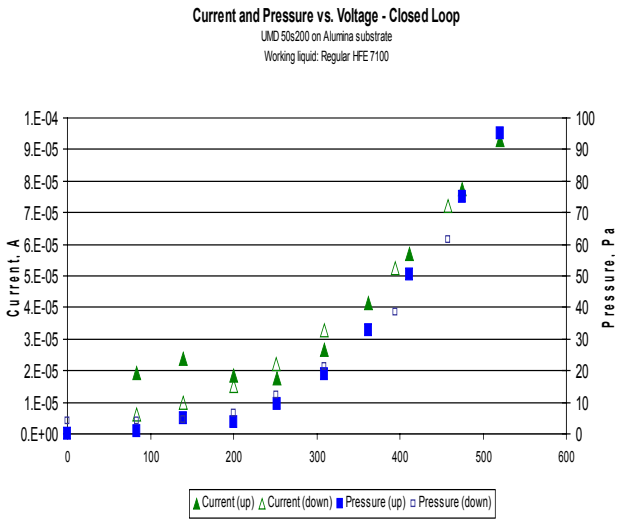


Fig. 16. Ion-drag pump test results [31]: Current (A) and pressure head (Pa) versus voltage (V) on x-axis

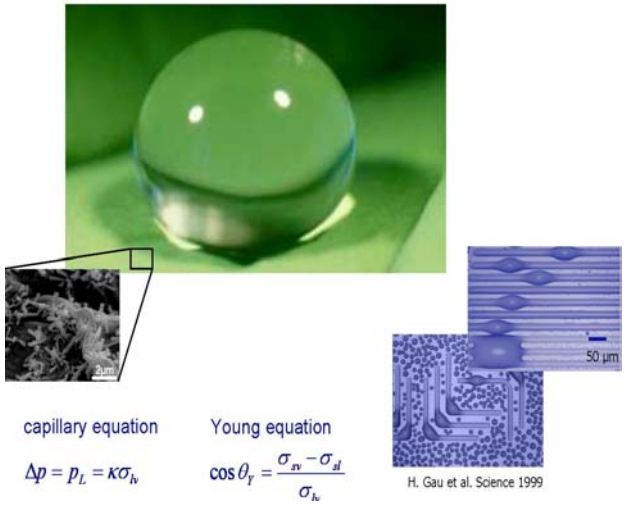


Fig. 17. Wetting and liquid micro-droplets: Liquid droplet on super-hydrophobic plant surface: "Lotus-effect"

**Electro-Wetting pumping and control issues**

The physical principle of electric wetting (EW) is to control the contact angle of a conductive liquid on an insulating surface, by control of the voltage between the liquid and an electrode embedded in the surface [32-36]. Using dedicated electrode configurations, droplets can be moved along pre-defined paths on the surface, liquid micro-structure morphology can be controlled to generate small droplets or to control the liquid in (micro-) channels, e.g. VCHP wick structures or in capillary structures at evaporator entrances of two-phase heat transport systems. The author of the current paper envisages several promising spacecraft TC applications.

Figure 17 illustrates properties of liquid microstructures in mechanical equilibrium. At small length scales, gravity is negligible (in space obviously even on large scales). Consequently the structure of liquid structures is entirely controlled by the requirements of constant mean curvature k, as required by the capillary equation, and by the Young equation, which relates the contact angle θ to the interfacial tensions $\sigma_{sl}$ (solid-liquid), $\sigma_{sv}$ (solid-vapour), $\sigma_{lv}$ (liquid-vapour)). For chemically, and/or topographically structured, surfaces this boundary condition at the substrate surface can give rise to rather complex liquid morphologies, as it is shown in the figure.

Figure 18 illustrates the basic principle of EW. By applying a voltage U between a partially wetting conductive liquid drop and an insulator covered electrode on the substrate, the contact angle can be reduced in such a way that the cosine of the contact angle increases quadratic with U, as expressed by the EW-equation (Fig. 18). This figure shows experimental data for a water drop on a Teflon surface immersed in a silicone oil bath. Note the perfect reversibility.

The author of this paper already identified three examples of possible EW applications in aerospace TC systems. The first one is illustrated by Figure 19, adapted from [36], showing EW-usage for loop cooling purposes. It deals with filling of groves, induced grooves, induced by EW.

The silicon substrate is covered with a thin oxide layer, which is hydrophobized with a self-assembled mono-layer. A liquid drop, deposited on the substrate, initially avoids the grooves. Upon applying a voltage, the contact angle decreases on the substrate. Due to the specific groove geometry,

the liquid suddenly fills the channels above a certain threshold voltage. When the voltage is reduced back to zero, the channels become empty again. Using pure electric control it is thus possible to fill and to empty the grooves reversibly. Given the large surface to volume ration of the grooves, meaning a very efficient heat transfer, this principle allows for an efficient, fully controllable cooling, e.g. for electronic chips in different equipment for terrestrial and aerospace applications.

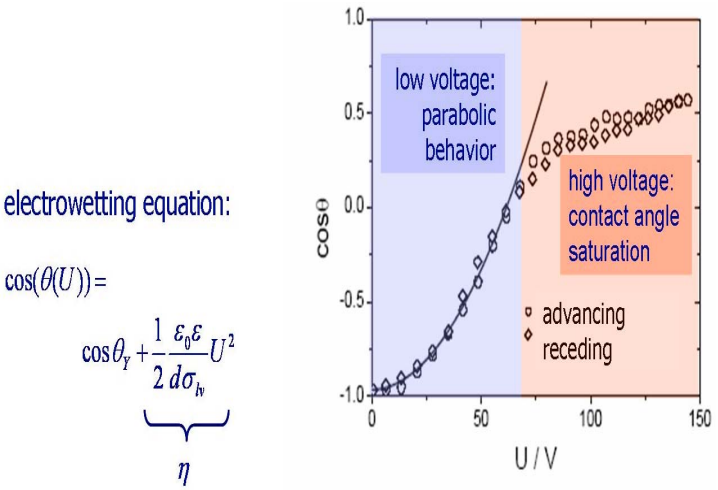


Fig. 18. EW-equation & EW-curve: Contact angle as a function of applied voltage

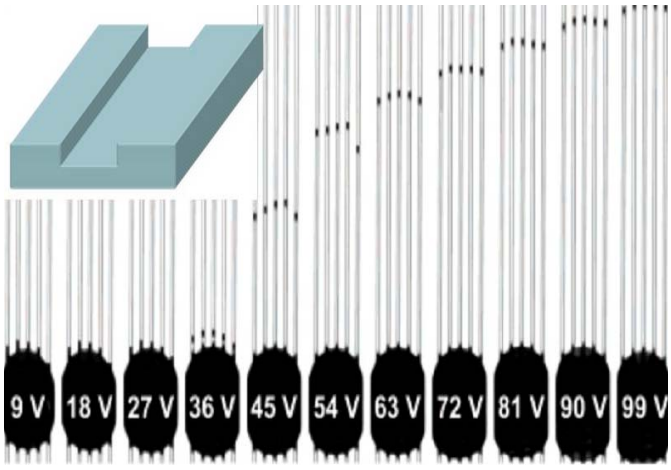


Fig. 19. EW-induced filling of grooves on a Si surface

Manipulating voltages of neighbouring electrodes is the baseline for two other EW applications.

Figure 20 shows that EW-induced droplets motions (by voltage manipulations) can be used to change the thermo-optical properties of a display. This can be used in variable coated solar panels and in space radiators. Figure 21 shows EW digital micro-fluidics applications attractive for mixing species in e. g. the pharmaceutical industry, but also attractive as a heat exchanger by controlled mixing parts of a working fluid (in TC systems in space), having different temperatures.

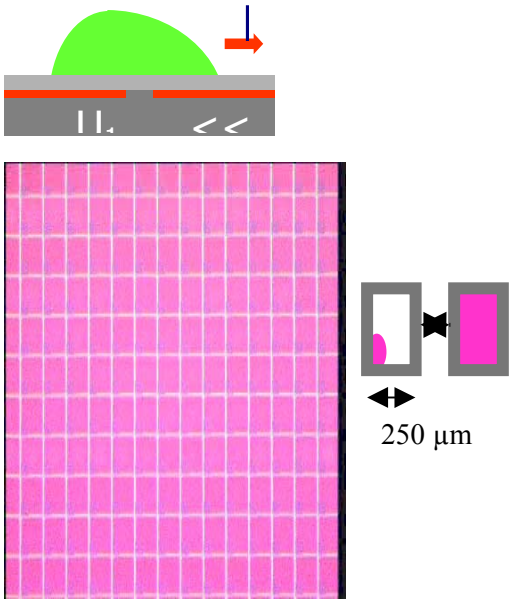


Fig. 20. EW-Display of R. Hayes

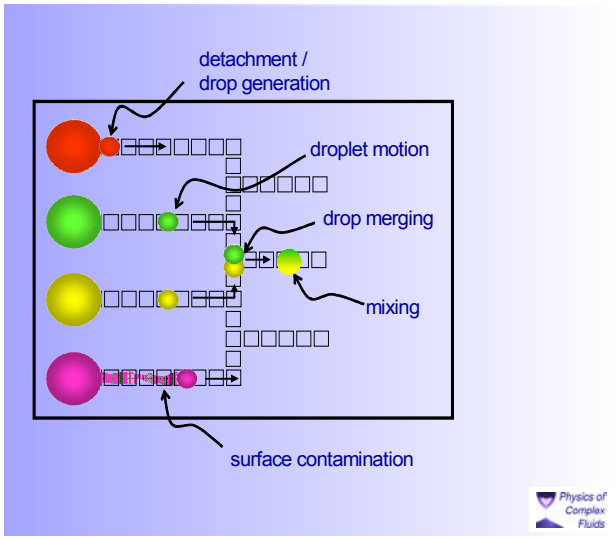


Fig. 21. EW for digital micro-fluidics applications

**Rotating radial heat pipe joint**

Details of the rotating radial heat pipe joint, and its proof of concept, are discussed in detail in [37–40]. This joint is a fully controllable rotating thermal joint for accurate positioning of spacecraft thermal radiators. The joint will be a promising alternative for the standard flexible thermal joints.

**Planetary thermal & environmental issues**

The information presented in the NASA-Goddard figures 22–26 [41, 42] can be summarised by the following:

– Thermally & environmentally is the “Moon a harsh mistress”: Heat rejection during the day and warmth maintenance during night, uneven thermal loading, partial gravity (~16% of Earth-g), and dust issues.
– Mars & Moon environments are different: The Moon is not a direct analogue of Mars, since Mars has a 6–12 torr. carbon-dioxide atmosphere and ~ 40% of Earth-g.

The maybe even crucial issue of the dust problem on Moon and Mars. This because dust and its negative effects for TC surfaces, mechanisms, EVA operations, and for planetary bases, constitutes a serious problem, to be attacked as soon as possible.

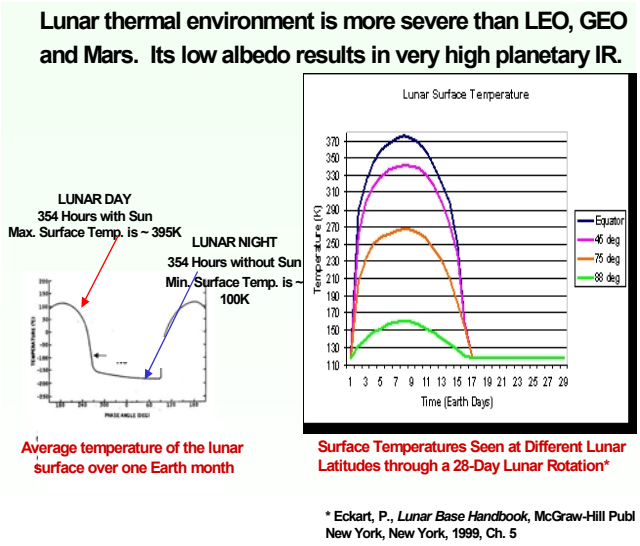


Fig. 22. Lunar surface thermal environment [42]

The concept of NASA-Goddard’s ”Dusty Environmental Effects Particle” (DEEP) chamber is shown in Figure 25.

- **Planetary temperature extremes yield design challenges**
  - Require to ***design for extremes***; CTE effects, need for modulation.
  - Heat rejection during the day, warmth maintenance at night
  - ***Uneven thermal loading*** from simultaneous exposure to radically different thermal sinks (e.g., direct sun to shadows in craters or from equipment)
- **Partial gravity environment**
  - Should yield similar results to earth, but in-situ demos will be needed for critical fluid-based thermal subsystems
- **Unknowns of Lunar/planetary environment**
  - ***Dust*** is a major issue for thermal and PV surfaces, movable joints, EVA hazard, etc.
  - Micrometeoroids, combined radiation/thermal effects, etc
  - ***A Lunar LDEF needed?***
- **Mars environment is different, Moon not a direct analogue**
  - Thin CO2 atmosphere, convection/conduction a significant issue; dust storms; lower direct solar radiation (overall about 42% of Earth gravity)
  - Modeling and test simulation issues

Fig. 23. Environmental facts for Moon & Mars [42]

- **Martian $CO_2$ atmosphere (6 – 12 torr) presents an analysis challenge due to gas conduction and convection, at 3/8$^{th}$ G**
  - Traditional spacecraft thermal analysis software is not able to model these effects, and CFD tools are being added in
  - MLI performs very poorly ($CO_2$ gas causes thermal short)
- **Dusty environment**
  - Atmosphere Tau (optical depth) can vary from 0.2 to 3.0
  - Dust on radiators, *may* be removed by random "dust devils
- **Diurnal, seasonal & location changes in thermal environment**
- **Rover thermal environment changes as MSL traverses landscape**
- **Performance of heat pipes will depend upon orientation**
  - Rover tilt up to 30°, but pipes are in a 3/8$^{th}$ G environment

Fig. 24. Thermal issues unique to Mars [42]


Fig. 25. NASA-Goddard's Dusty Environmental Effects Particle (DEEP) chamber [42]

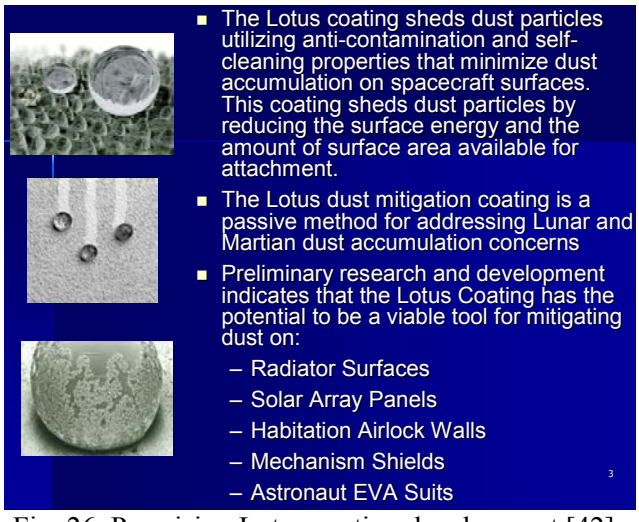


Fig. 26. Promising Lotus coating development [42]

## CONCLUDING REMARKS

Concerning Moon & Mars applications, this paper not only updates/extends relevant thermal-gravitational approach and supporting research issues. [2]). It adds and discusses also some important research items to be looked at als, e.g.:

- JPL's Magnetic Levitation facility (Maglev).
- The application possibilities and merits of currently available Electro-Osmotic pumps for two-phase loop control operation and control.
- Electro wetting fluid manipulation issues for aerospace applications.
- NLR's rotating radial heat pipe joint (a promising alternative for classical flexible thermal joints).
- Problematic Moon and Mars environmental issues, and the way to solve dust and atmospheric problems, by experimenting in the Dusty Environmental Effects Particle (DEEP) chamber and, if possible, in a lunar Long Term Exposure Facility (LDEF) to develop dust removing surfaces and coatings, by the creation of novel spacecraft thermal analysis software to tackle the effects of gas conduction and convection.
- Solving the effects of partial gravity by earth based modelling and testing, i.e. via the described thermal-gravitational modelling and scaling approach, of which the results are to become credible by in-situ demos.
- It is considered worthwhile and cost effective to fly pre-cursor two-phase TC loops as hitchhiker to a Moon or Mars lander (e.g. the International Mars Sample Return Mission [43]) to leave it there and monitor the performance from the earth.

The target of this paper, i.e. to plan one of the important key technologies needed for future planetary exploration, i.e. the creation of thermal management systems for Moon and Mars base household (habitability) and science applications, is detailed in a straightforward way.

## References


1. Moore, C., Thermal management technology for exploration, International Two-Phase Thermal Control Workshop, Johns Hopkins University/APL, Laurel, USA, Sept. 2006.
2. Delil, A.A.M., Planetary Two-Phase Thermal Control Systems Design Using Terrestrial Test Data from Model Systems, Built According to Thermal-Gravitational Modelling and Scaling Laws, SAE- 2007-01-3242, 37th Int. Conf. on Environmental Systems, Chicago, USA, July 2007, *SAE Trans., J. Aerospace,* 107, 2007.
3. Delil, A.A.M., Thermal gravitational modelling and scaling of two-phase heat transport systems: Similarity considerations and useful equations, predictions versus experimental results, NLR TP 91477, 1st European Symposium Fluids in Space, ESA SP-353, 579-599, Ajaccio, France, 1991.
4. Delil, A.A.M., Two-phase heat transport systems for spacecraft – Scaling with respect to gravity, NLR TP 89127, SAE 891467, 19th Intersociety Conference on Environmental Systems, San Diego, USA, July 1989, *SAE Trans., J. Aerospace*, 98, 1989, 554-564.
5. Delil, A.A.M., On Thermal-Gravitational Modelling, Scaling and Flow Pattern Mapping Issues of Two-Phase Heat Transport Systems, NLR-TP-98268, SAE 981692, 28th Int. Conference on Environmental Systems, Danvers, USA, July 1998, *SAE Trans., J. Aerospace,* 107, 1998.
6. Delil, A.A.M., Microgravity two-phase flow and heat transfer, NLR-TP-99429, *Chapter 9 of Fluid Physics in Microgravity*, Monti, R. (Ed.), Gordon and Breach Science & Harwood Academic Publishers, Reading, UK, 2002.
7. Delil, A.A.M., Thermal-Gravitational Modelling and Scaling of Heat Transport Systems for Applications in Different Gravity Environments: Super-Gravity Levels & Oscillating Heat Transfer Devices, NLR-TP-2000-213, SAE-2000-01-2377, Proc. 30th Int. Conf. on Environmental Systems, Toulouse, France, July 2000, *SAE Trans. Journal of Aerospace*, 2000.
8. Miller Hurlbert, K., *Flow Dynamics for Two-Phase Flows in Partial Gravities*, PhD Thesis, University of Houston, USA, 2000.
9. Murphy, G., *Similitude in Engineering,* Ronald Press, New York, USA, 1950.

10. Delil, A.A.M., Results of Thermal-Gravitational Modelling and Scaling of Two-Phase Heat Transport Systems for Moon and Mars Applications: Results for Different Working Fluids, submitted for ASME Int. Mechanical Engineering Congress & Exposition - Boston, USA, November 2008.
11. Oshinowo, T., Charles, M.E., Vertical Two-Phase Flow, Flow Pattern Correlations, *Can. J. Chem. Engng*., 52, 1974, pp. 25-35.
12. Delil, A.A.M., Gravity dependence of pressure drop and heat transfer in straight two-phase heat transport system condenser ducts, NLR-TP-92167, SAE 921168, 22nd Int. Conf. on Environmental Systems, Seattle, USA, July 1992, *SAE Trans., J. Aerospace,* 101, 1992, pp. 512-522.
13. Delil, A.A.M., Gravity dependent condensation pressure drop and heat transfer in ammonia two-phase heat transport systems, NLR-TP-92121, AIAA 92-4057, National Heat Transfer Conf., San Diego, USA, July 1992.
14. Soliman, M. & Schuster, J.R., Berenson, P.J., A General Heat Transfer Correlation for Annular Flow Condensation, *ASME C, J. Heat transfer,* 1968, 90, pp. 267-276.
15. Zivi, S.M., Estimation of Steady-State Void Fraction by Means of the Principle of Minimum Entropy Production, *Trans. ASME C, J. Heat Transfer*, 1964, 86, pp. 247-252.
16. Da Riva, I., Sanz. A, Condensation in Ducts, *Microgravity Science & Technology*, 4**,** 1991, 179-187.
17. Delil, A.A.M. et al., TPX for In-Orbit Demonstration of Two-Phase Heat Transport Technology - Evaluation of Flight & Postflight Experiment Results, NLR-TP-95192, SAE 95150, 25th Int. Conf. on Environmental Systems, San Diego, USA, July 1995.
18. Carey, P., *Liquid-Vapor Phase-Change Phenomena*, Hemisphere Publ. Cy, Washington DC, USA, 1992.
19. Hamme, T.A., Best, F.R., Gravity Dependent Flow Regime Mapping, AIP Conf. Proc. 387, *Space Technology & Applications International Forum*, Albuquerque, USA, 1997, pp. 635-640.
20. Wallis, G.B., *One-dimensional Two-phase Flow*, McGraw-Hill, New York, 1969.
21. Tamburini, P., "T-System", Proposal of a New Concept Heat Transport System, 3rd Int. Heat Pipe Conference, Palo Alto, USA, July 1978, AIAA CP-784, pp. 346-353.
22. Lund, K.O., Baker, K.W., Weislogel, M.M., The Vapor-Pressure Pumped Loop Concept for Space Systems Heat Transport, (*Proc. 1st Int. Conference on Aerospace Heat Exchanger Technology 1993,* Palo Alto, CA, USA, (Eds. Shah, R.K., Hashemi, A.), Elsevier, Amsterdam 1993, pp. 45-55.
23. Borodkin, A.A., Kotlyarov, E.Yu., Serov, G.P., Evaporation-Condensation Pump for Providing of Working Fluid Circulation in Two-Phase Heat Transferring System, SAE 951508, 25th Int. Conf. on Environmental Systems, San Diego, USA, July 1995.
24. Liu, Y, et al., Variable Gravity Simulation by Maglev, Proc. Int. Two-Phase Thermal Control Workshop, Laurel, USA, Sept. 2006.
25. Delil, A.A.M., Mugele, F., Reappraisal of Unrealised and Novel Thermal Control Issues for Applications in Future Spacecraft, SAE2006-01-2230, 36th Int. Conf. on Environmental Systems, Norfolk, USA, July 2006.
26. Delil, A.A.M., Advanced thermal control systems for future space science missions and Mars or lunar base household and research, International Two-Phase Thermal Control Workshop, Laurel, USA, Sept. 2006.
27. Delil, A.A.M., Unrealised Thermal Control Issues Important for Future Spacecraft Thermal Control Systems Design, AIAA-2007-1212, 45th AIAA Aerospace Sciences Meeting and Exhibit, Reno, USA, Jan. 2007.
28. Delil, A.A.M., Advanced Thermal Control for Future Space Science Missions or Mars & Lunar Base Household and Research, P1: TC Issues deserving more attention, P2: Restarted development and novel research issues, *Conf. on Thermophysics in Microgravity, Space Technology & Applications International Forum*, Albuquerque, USA, Feb. 2007.
29. Delil, A.A.M., Fully controllable heat pipe with a short electro-osmotic pumping section, NLR MP 82049, AIAA-83-317, AIAA Aerospace Sciences Meeting, Reno, USA, Jan. 1983.
30. Yao, S., et al., A large flow-rate electro-osmotic pump with micro-pores, *Proc. 2001 ASME IMECE*, Nov. 2001, New York.
31. Didion, J., Advancements in ElectroHydroDynamic (EHD) Thermal Control Systems, 15th Spacecraft Thermal Control Workshop, El Segundo, USA, 2005.

32. Mugele, F., et al., Electrowetting: A convenient way to switchable wettability patterns, *J. Physics: Condensed Matter*, 17, 2005, pp. 559-576.
33. Mugele, F. Baret, J.C., Electrowetting from basics to applications, *J. Physics: Condensed Matter*, 17, 2005, pp. 705-774.
34. Baret, J.C., *Morphological Transitions in Simple Electrocapillary/Systems Tools for Microfluidic Liquid Manipulation*, PhD thesis University Twente, The Netherlands, 2005.
35. Baret, J.C., et al., Electro-actuation of Fluid using Topographical Wetting Transitions, *Langmuir*, 21, 12218, 2005.
36. Baret, J.C., Mugele, F., Electrical discharge in capillary break-up: controlling the charge of a droplet, *Physical Review Letters,* 96, 016106, 2006.
37. Delil, A.A.M., "Considerations concerning a thermal joint for a deployable of steerable radiator for the Columbus Polar Platform", NLR TR 86055 U, 1986.
38. Delil, A.A.M., Moveable thermal joints for deployable or steerable spacecraft radiator systems, NLR MP 87016, SAE 871460, 17th Intersociety Conference on Environmental Systems, Seattle, USA, July 1987.
39. Delil, A.A.M., et al., Sensors and Components for Aerospace Thermal Control and Propellant Systems, NLR TP 97282 U, ESA-SP-400, 6th European Symp. on Space Environment Control Systems, Noordwijk, Netherlands, May 1997, pp. 289-297 and SAE 972478, 27th Int. Conference on Environmental Systems, Lake Tahoe, USA, July 1997.
40. Delil, A.A.M., et al., Sensors and Components for Aerospace Thermal Control, Life Science and Propellant Systems, NLR TP 97504 L, *AIP Proc. 2nd Conference on Applications of Thermophysics in Microgravity, Space Technology & Applications International Forum*, Albuquerque, USA, Feb. 1998.
41. Swanson, T., Butler, D., NASA/Goddard Thermal Control Road Map, Proc. 18th Aerospace Spacecraft TC Workshop, El Segundo, March 2007.
42. Swanson, T., Butler, D., NASA/Goddard Thermal Control Road Map, Proc. 19th Aerospace Spacecraft TC Workshop, El Segundo, March 2008.
43. Report for the International Mars Architecture for the Return of Samples (iMARS) Working Group Conference, Paris, France, 9 -10 June 2008.

**ACRONYMS & NOMENCLATURE**

| | |
|---|---|
| CPL | Capillary Pumped Loop |
| DEEP | Dusty Environmental Effects Particle |
| EHD | Electro-Hydro-Dynamic(s) |
| EO | Electro-Osmosis (-Osmotic) |
| EW | Electro-wetting |
| FOM | Figure of Merit |
| HP | Heat Pipe(s) |
| LDEF | Long Duration Exposure Facility |
| LHP | Loop Heat Pipe(s) |
| MPL | Mechanically Pumped Loop(s) |
| NLR | (Dutch) National Aerospace Laboratory |
| TC | Thermal Control |
| VCHP | Variable Conductance Heat Pipe(s) |
| VPDL | Vapour Pressure Driven Loop(s) |

**NOMENCLATURE**

| | |
|---|---|
| A | area ($m^2$) |
| B, A, | equivalent thermal conductance (W/m K) |
| Bo | boiling number or Bond number (-) |
| $C_p$ | specific heat at constant pressure ($J.kg^{-1}. K^{-1}$) |
| $C_v$ | specific heat at constant volume ($J.kg^{-1}. K^{-1}$) |
| D | diameter (m) |
| d | hydraulic diameter or thickness (m) |
| E | electric field strength (V/m) |
| Eu | Euler number(-), |
| F | force (N) |
| Fr | Froude number (-) |
| f | friction factor (-) |
| g | acceleration ($m\ s^{-2}$) |
| H | coupling factor ($m^3.s^{-1}.V^{-1}$), enthalpy ($J.kg^{-1}$) |

h heat transfer coefficient (W $m^{-2}$ $K^{-1}$)
$h_{lv}$ latent heat of vaporisation (J $kmol^{-1}$ $K^{-1}$)
I current (A)
K permeability ($m^2$)
L length (m)
M molecular weight ($kg.kmol^{-1}$)
Ma Mach number (-)
Mo Morton number (-)
$N_{eo}$ electro-osmotic FOM (-)
$N_g$ gravity FOM (-)
$N_l$ 0-g FOM, liquid transport factor (W $m^{-2}$)
$N_p$ 1-g or pumping FOM, wicking height ($m^2$)
$N_r$ transport capability reduction factor (-)
$N_w$ wick FOM, wick number ($m^2$)
$N_S$ gas control sensitivity factor (K)
Nu Nusselt number (-)
Pr Prandtl number (-)
p pressure (N $m^{-2}$)
Q power, heat load/throughput (W)
R radius (m)
R flow/thermal resistance (N.s.$m^{-5}$/ .$W^{-1}$)
$R_0$ universal gas constant (J $K^{-1}$ $kmol^{-1}$)
$R_e$ electric resistance (Ω)
Re Reynolds number (-)
S slip factor (-)
T temperature (K, °C)
V volume ($m^3$)
U, V voltage (V)
U, v velocity (m $s^{-1}$)
We Weber number (-)
X vapour quality (-)
x axial co-ordinate (m)
z axial co-ordinate (m)

Greek
α $K.r^{-2}$, void fraction (-)
β shape or flow profile factor (-)
γ power enhancement factor (-)
γ' radial-axial momentum transition factor
Δ delta, difference (-)
ε porosity (-), or $\varepsilon_0$. $\varepsilon_r$ ($A^2.s^4.kg^{-1}$ $m^{-3}$)
$\varepsilon_0$ dielectric constant of vacuum ($A^2.s^4.kg^{-1}$ $m^{-3}$)
$\varepsilon_r$ relative electric permittivity (-)
Φ volumetric flow ($m^3.s^{-1}$)
λ electric conductivity of surface ($\Omega^{-1}$)
μ viscosity (N.s $m^{-2}$)
ρ density ($kg.m^{-3}$)
σ surface tension (N.$m^{-1}$, J. $m^{-2}$),
$\lambda_l$ electric conductivity of liquid ($\Omega^{-1}$ $m^{-1}$)
θ contact angle/inclination with g-vector (degr.)
ζ electro-osmotic potential (V)

Subscripts
A, a adiabatic section
C, c condenser
E evaporator
e electric, evaporator
f front
g gas